

Charge transport in functionalized multi-wall carbon nanotube-Nafion composite

C. S. Suchand Sangeeth, R. Kannan, Vijayamohan K. Pillai, and Reghu Menon

Citation: *J. Appl. Phys.* **112**, 053706 (2012); doi: 10.1063/1.4749264

View online: <http://dx.doi.org/10.1063/1.4749264>

View Table of Contents: <http://jap.aip.org/resource/1/JAPIAU/v112/i5>

Published by the [American Institute of Physics](#).

Related Articles

Autonomic restoration of electrical conductivity using polymer-stabilized carbon nanotube and graphene microcapsules

[Appl. Phys. Lett.](#) **101**, 043106 (2012)

Electron transport in suspended semiconductor structures with two-dimensional electron gas

[Appl. Phys. Lett.](#) **100**, 181902 (2012)

Single-layer behavior and slow carrier density dynamic of twisted graphene bilayer

[Appl. Phys. Lett.](#) **100**, 091601 (2012)

Growth and surface potential characterization of Bi₂Te₃ nanoplates

[AIP Advances](#) **2**, 012114 (2012)

Electron tunneling through atomically flat and ultrathin hexagonal boron nitride

[Appl. Phys. Lett.](#) **99**, 243114 (2011)

Additional information on *J. Appl. Phys.*


Journal Homepage: <http://jap.aip.org/>

Journal Information: http://jap.aip.org/about/about_the_journal

Top downloads: http://jap.aip.org/features/most_downloaded

Information for Authors: <http://jap.aip.org/authors>

ADVERTISEMENT



Special Topic Section:
PHYSICS OF CANCER

Why cancer? Why physics? [View Articles Now](#)

Charge transport in functionalized multi-wall carbon nanotube-Nafion composite

C. S. Suchand Sangeeth,^{1,a)} R. Kannan,² Vijayamohan K. Pillai,² and Reghu Menon¹

¹*Department of Physics, Indian Institute of Science, Bangalore 560012, India*

²*Physical and Materials Chemistry Division, National Chemical Laboratory, Pune 411008, India*

(Received 2 May 2012; accepted 31 July 2012; published online 5 September 2012)

The charge transport in sulfonated multi-wall carbon nanotube (sMWNT)-Nafion composite is reported. The scanning electron microscope images of the composite, at 1 and 10 wt % of sMWNT, show that the nanotubes are well dispersed in polymer matrix, with conductivity values of 0.005 and 3.2 S/cm, respectively; and the percolation threshold is nearly 0.42 wt. %. The exponent (~ 0.25) of the temperature dependence of conductivity in both samples indicates Mott's variable range hopping (VRH) transport. The conductance in 1 wt. % sample increases by three orders of magnitude at high electric-fields, consistent with VRH model. The negative magnetoresistance in 10 wt. % sample is attributed to the forward interference scattering mechanism in VRH transport. The ac conductance in 1 wt. % sample is expressed by $\sigma(\omega) \propto \omega^s$, and the temperature dependence of s follows the correlated barrier hopping model. © 2012 American Institute of Physics.

[<http://dx.doi.org/10.1063/1.4749264>]

I. INTRODUCTION

Among several types of carbon nanotube (CNT)—polymer composites, the composites with speciality polymers like Nafion for applications in fuel cells, actuators, etc., are yet to be investigated thoroughly.^{1–3} Although CNT-Nafion composite membranes have shown enhanced actuator characteristics than the usual metal filled Nafion membranes, the role of nanomorphology in charge transport is not very well understood.¹ It is known that subtle variations in the dispersion of CNTs in polymer matrix can substantially alter the physical properties, and in special polymers like Nafion to attain a homogenous distribution of CNT remains a challenge.² This is mainly due to the fact that the debundling of CNTs does not occur that easily and the processing conditions for both CNTs and polymer should be compatible to facilitate uniform dispersion of CNTs.

Earlier studies in CNT-polymer composites have shown that electrical transport properties are quite sensitive to the extent of dispersibility of CNTs in polymer matrix.⁴ However, the measurements around room temperature are not adequate enough to determine this correlation, since the thermally activated processes could smear out the subtleties in inter-tube transport. Although parameters like percolation threshold are shown to be sensitive to sort out the problems due to bundling, aggregation, and processing conditions, the wide variations in room temperature conductivity near percolation threshold suggest that low temperature transport data are required to identify the conduction mechanisms.^{5–7} Furthermore, wide range of values (from 0.1 to 10 wt. %) for the threshold of percolative transport has added more ambiguity to this scenario.^{8,9} Apart from these morphological issues, the electrical properties of CNT-polymer composites are quite often characterized only by the temperature de-

pendence of dc conductivity, and this has raised some concern that it is not possible to distinguish between various types of hopping and tunnelling mechanisms in complex systems.¹⁰ These shortcomings can be addressed by a comprehensive study of conductivity as a function of temperature, frequency, electric-field, and magnetic field, as has been carried out in CNT-Nafion composites in this work, to improve the understanding on how nanoscale variations in CNT network affect the bulk transport.

It is known that a better interface between polymer chains and CNT helps to enhance the physical properties. Since debundling and dispersing individual tubes are not trivial, the functionalization of the sidewalls of CNTs can overcome some of these problems.⁴ The sidewalls of CNTs functionalized with sulfonic acid groups tend to prevent the formation of large sized aggregates.^{2,11} The effective chemical interaction between the sulfonic acid moieties on the sidewalls with Nafion also enhances the hydrophilic type interactions that help in the formation of well dispersed composites.¹² The sulfonic acid groups enhance the proton transport through Nafion membrane by forming proton conductive clusters.^{2,12} Further, the individually functionalised multi-wall carbon nanotubes (MWNTs) significantly improve the interfacial bonding between the MWNTs and Nafion and thereby enhancing the mechanical properties of the membrane.¹³ In this facile processing technique, it is possible to substantially increase the amount of well-dispersed CNTs in polymer matrix. In such a well-dispersed network of individual tubes, the inter-tube transport is expected to be better.

In this report, transport properties of sulfonated multi-wall carbon nanotube (sMWNT)-Nafion composites (1 and 10 wt. % of sMWNT) have been carried out as a function of temperature, high electric-field, high frequency, and also high magnetic field, to investigate the role of network connectivity in charge transport. The percolation threshold is observed to be around 0.42 wt. % of sMWNT. The room temperature

^{a)}E-mail: suchandsangeeth@gmail.com.

conductivities of 1 and 10 wt. % samples are 0.005 and 3.2 S/cm, respectively; and the temperature dependence of conductivity of latter is rather weak, although both samples show three-dimensional (3D) Mott variable range hopping (VRH) transport. This is observed to be consistent with the results from electric-field and magnetoresistance (MR) measurements. The frequency dependent transport indicates that the onset frequency for the increase in conductance is varied by nearly four orders of magnitude. AC conductance follows a power law $\sim \omega^5$ and the temperature dependence of the exponent suggests that correlated barrier hopping (CBH) model is quite appropriate.

II. EXPERIMENTAL

The MWNTs are acquired from Chemapol industries Pvt. Ltd, Mumbai, India and are of >90% purity. These MWNTs were further treated in 11 M HCl at 100 °C for 1 h to remove any metallic impurities that might be present. sMWNTs were prepared by treating 100 mg of MWNTs with a mixture of concentrated nitric acid and sulphuric acid (15 ml each) under microwave power of 540 W.¹² The XPS measurements on sMWNT revealed the absence of any metal impurities [see supplementary information,³⁵ Fig. 1]. After microwave treatment, the mixture was refluxed with concentrated hydrochloric acid (30 ml) for 1 h and then filtered through a 200 μm poly-tetrafluoroethylene (PTFE) membrane. This acid treated MWNTs were dried in an oven overnight and stored in an airtight container. The composite membrane fabrication is reported elsewhere.¹² Appropriate amount of sMWNTs and pre-casted Nafion membranes were mixed with 18 ml of dimethyl acetamide, and stirred for 4 h at 60 °C, and further sonicated for 2 min. Free standing films (the thickness of 10 wt. % film is 40 μm , whereas the lower wt. % samples were of 90–130 μm thick film) of sMWNT-Nafion were prepared by solution casting, and drying at 80 °C for 24 h, followed by annealing at 150 °C under vacuum for 2 h. These films are peeled off from the substrate and used for charge transport measurements.

Four-terminal resistance measurements were carried out from 300 to 4.2 K in a Janis continuous flow cryostat. The dc conductivity measurements are performed with a constant current sourced through a current source (model Keithley-220) and the voltage measured through an electrometer (model Keithley-6514). The current values were typically in the range of 20–100 nA, chosen to avoid any sample heating at low temperatures. The high electric-field characteristics

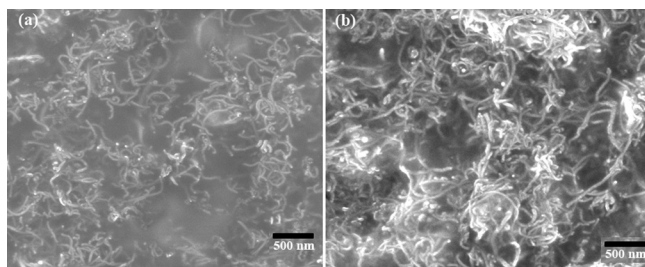


FIG. 1. Scanning electron microscope images of sulfonated MWNT-Nafion composites: (a) 1 wt. % sMWNT and (b) 10 wt. % sMWNT loading.

were measured by using a pulsed four-probe technique, as described elsewhere.¹⁴ Magnetoresistance measurements were performed in Janis variable-temperature superconducting magnet system, up to 11 T and temperatures down to 4.2 K. For the magnetoresistance measurement, the current is sourced using Keithley 220 current source and the voltage measured by Keithley 2000 multimeter. The ac conductivity of the composites is measured from 100 Hz to 16 MHz using an Agilent 4294 A precision impedance analyzer.

III. RESULTS AND DISCUSSIONS

The morphology of the composite films (1 and 10 wt. % sMWNT loading) can be observed from the scanning electron microscope (SEM) images, as shown in Fig. 1. The contrast among these two images clearly shows that the density of the network increases with sMWNT filling. Since Nafion membrane is often used in fuel cells, it is important to find out the optimal loading, which at the same time yields adequate porosity in the network to enable efficient mass transport of ions. The SEM image of 10 wt. % filling does not show any severe aggregation related issues as usually observed in MWNT-polymer composites. This is mainly due to the functionalization of MWNTs that enhances a fairly uniform dispersion within the polymer matrix. Although the charge transport properties in several MWNT-polymer systems are investigated, there are only a few transport measurements in well-dispersed MWNT networks in polymer matrix.¹⁰

The conductivity (σ) as a function of sMWNT weight percentages (p) is shown in Fig. 2. The electrical conductivity of the sulfonated MWNT-Nafion composite is much larger than the value reported for other MWNT-modified Nafion membranes, which could be due to the better dispersion of sMWNTs.^{15,16} The sharp increase in conductivity at a weight fraction of $p \sim 0.42$ indicates the onset of the threshold for percolative transport, and the tendency to saturate at larger values of p suggests that the conductivity follows the well known scaling law for percolation: $\sigma \propto (p - p_c)^t$; where p_c is the percolation threshold, and the exponent t depends on sample dimensionality.¹⁷ A fit to this

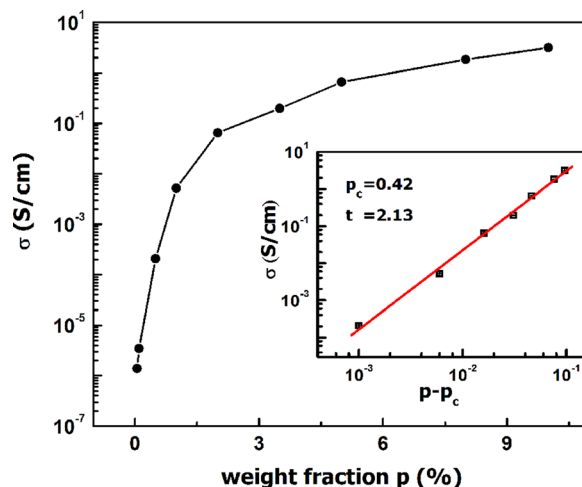


FIG. 2. dc conductivity vs. weight fraction of sMWNT at 300 K. Inset shows the linear fit to the scaling law of percolation.

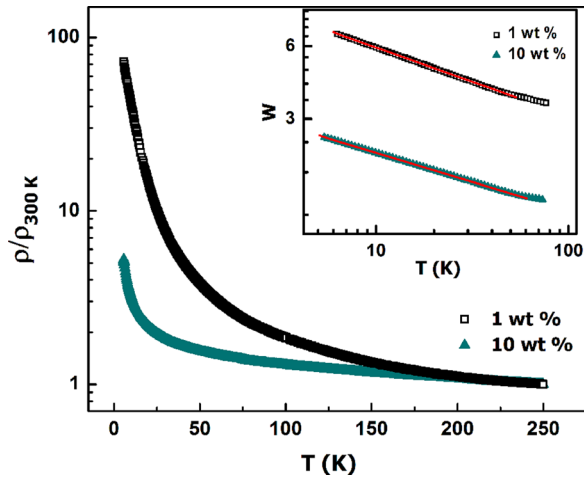


FIG. 3. Normalized resistivity vs. temperature for 1 and 10 wt. % sMWNT-Nafion composites. Inset shows the reduced activation energy [W vs. T] plot on a log-log scale.

scaling equation [see inset of Fig. 2] gives $p_c \sim 0.42$ and $t \sim 2.13$, in agreement with the predicted value of $t \sim 2$ for percolation in 3D. As the weight percentage of sMWNT in composite increases, the density of network connections and the presence of multiple parallel resistors increase, and these reduce the bulk resistance.

The SEM images of 1 and 10 wt. % of sMWNT loaded samples show that the connectivity is quite rarefied at 1 wt. % and it gets denser at 10 wt. %. Hence, the transport properties of these two extremal cases are worth investigating, since the samples below 1 wt. % of sMWNT are highly resistive at low temperatures, and the samples in between 1 and 10 wt. % do not show any significant variations. The temperature dependence of the resistance of 1 and 10 wt. % sMWNT-Nafion is shown in Fig. 3. Although the resistance in both cases shows strong temperature dependence at $T < 50$ K, in case of 10 wt. % sample it is relatively weaker. The temperature dependence of resistance is fitted to the VRH model

$$R = R_0 \exp(T_0/T)^p, \quad (1)$$

where R_0 is characteristic of the sample and T_0 determines the thermal activation energy for hopping among localized states. The exponent p for hopping conduction for 1 and 10 wt. % samples is determined from the reduced activation energy $W(T) = -\partial \ln \rho / \partial \ln T$ plots, as in the inset of Fig. 3. The negative slope in W -plot shows that both samples are in the insulating regime at low temperatures. The values of p for 1 and 10 wt. % samples are 0.28 and 0.24, respectively, suggesting that both systems are close to Mott's 3D VRH. The values of T_0 for 1 and 10 wt. % samples are 38500 and 560 K, respectively. From these T_0 values, the localization length for 10 wt. % sample is estimated to be around four times larger than that of 1 wt. % sample.¹⁸ This shows that the connectivity and delocalization in 10 wt. % sample are considerably enhanced, as also supported by the high frequency and high electric-field transport studies presented below.

The electric-field dependence of conductance at different temperatures for 1 and 10 wt. % of sMWNT-Nafion

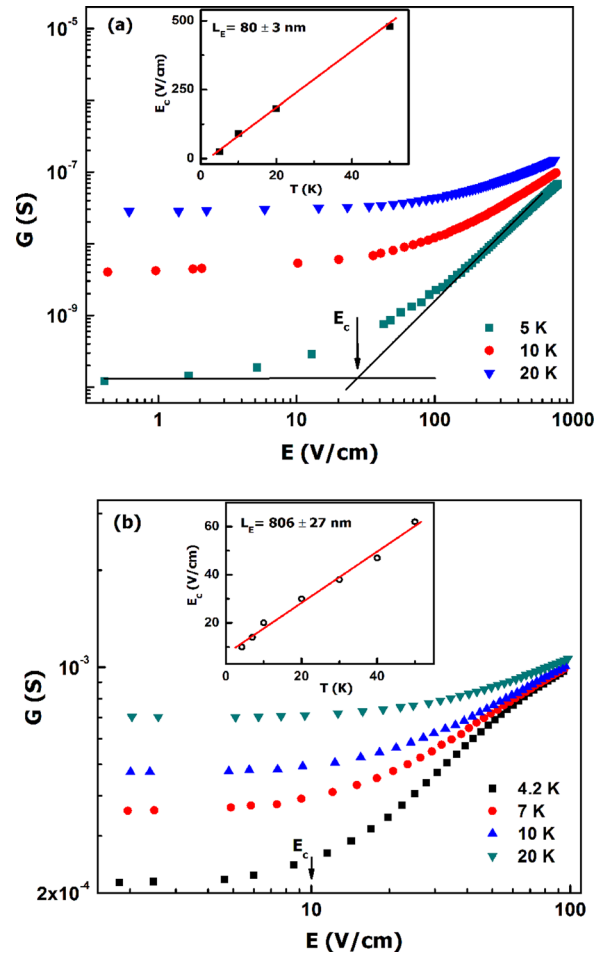


FIG. 4. (a) Conductance vs. electric-field for 1 wt. % sMWNT-Nafion sample. Inset shows the threshold field vs. T , with linear fit to Eq. (2). (b) Conductance vs. electric-field for 10 wt. % sample. Inset shows the threshold field vs. T , with linear fit to Eq. (2).

composites is plotted in Fig. 4. An Ohmic (i.e., field independent) conductance is observed at low electric-field, while beyond a critical threshold electric-field E_c , the conductance increases till it becomes nearly temperature independent. In 1 wt. % sMWNT sample, the conductance increases by three orders of magnitude [Fig. 4(a)], whereas it hardly varies an order of magnitude for 10 wt. % sample. At low fields, the carrier hopping is mediated via phonons; hence, the field dependence is weaker. In VRH transport, conductivity increases with electric-field, since energy levels are lowered in the direction of field, facilitating the carrier hops, provided the sites have an energy difference not greater than the drop in potential energy along the field.^{19,20} This can be easily observed from the values of threshold field for the onset of the increase in conductance. In 1 wt. % sample, the availability of states for the hopping transport is less so that higher threshold field is required for the enhancement in conductance. Whereas in 10 wt. % sample the threshold field is lowered by an order of magnitude due to the abundance of hopping sites. The threshold field values are extracted as described elsewhere.²¹ As shown in the inset of Figs. 4(a) and 4(b), the values of E_c at different temperatures are found to increase linearly with temperature. This is mainly due to the fact that the carrier delocalization increases with

temperature and electric-field.¹⁹ The threshold field increases with temperature, since higher fields are required to overcome the scattering contributions from phonons. Above the threshold field, the energy from field assists the hops between states, since $eER > W$, where R is the separation between two states and W is the thermal hopping energy. For 3D Mott VRH, the thermal hopping energy $W \sim R^{-3}$ and hopping distance $R \sim T^{-1/4}$ suggest a linear dependence of E_c on temperature.²² The values of E_c facilitate the determination of a transport length scale in such network systems²¹

$$L_E = \frac{k_B T}{e E_c}, \quad (2)$$

where L_E corresponds to the size of regions with good conductivity that varies with sMWNT loading, and eEL_E is the energy gained by the carrier from the electric-field. The values of the connectivity length scale (L_E) for 1 and 10 wt. % samples are 80 and 806 nm, respectively. The higher value of L_E shows enhanced transport properties in 10 wt. % composite.

The transverse MR data for 10 wt. % sample are shown in Fig. 5. The MR is negative at low temperatures (4.2–20 K). Conventionally, this type of negative MR is attributed to the suppression of quantum localization corrections to the Drude conductivity in systems near metal-insulator transition: i.e., negative MR in weak localization.²³ However, this interpretation must be consistent with a relatively weaker temperature dependence of conductivity, as usually observed in disordered metallic regime. The resistivity data in Fig. 3 show that this is not the case, hence the negative MR cannot be explained due to weak localization, as the temperature dependence of conductivity shows VRH transport. Alternatively, Nguyen *et al.* have shown that a negative MR in VRH regime can arise from the interference of direct paths during forward scattering.²⁴ The low field MR data (<4 T) show [see Fig. 5] linear magnetic field dependence as predicted by this model. However, at higher fields ($B > 9$ T) the negative MR at 4.2 K is less than that of 10 and 20 K due to the competing positive MR contribution from the usual wave function shrinkage

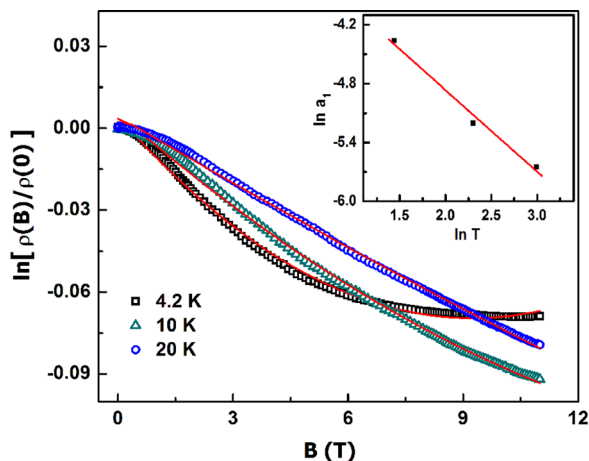


FIG. 5. Magnetoresistance vs. field for 10 wt. % sMWNT-Nafion composite at 4.2, 10, and 20 K. Solid lines are fit to Eq. (3). Inset shows the temperature dependence of the coefficient (a_1), as in Eq. (3).

effect in VRH transport.²⁵ The net MR by taking into account of the negative and positive contributions is given by the expression

$$\ln[\rho(B)/\rho(0)] = -a_1 B + a_2 B^2 + a_3, \quad (3)$$

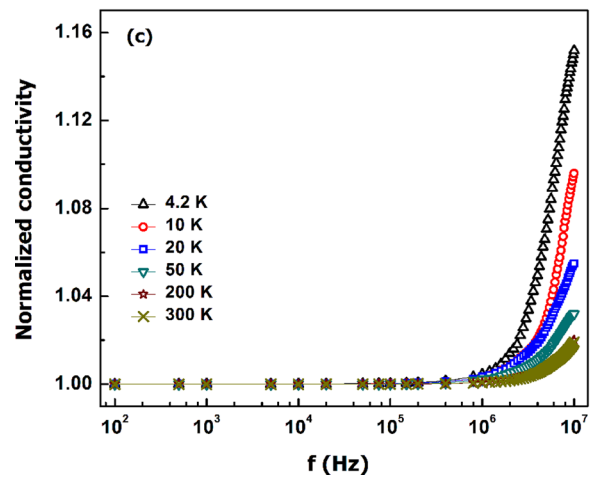
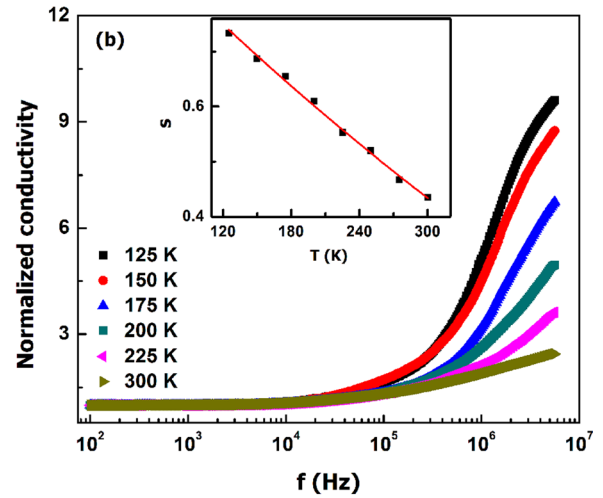
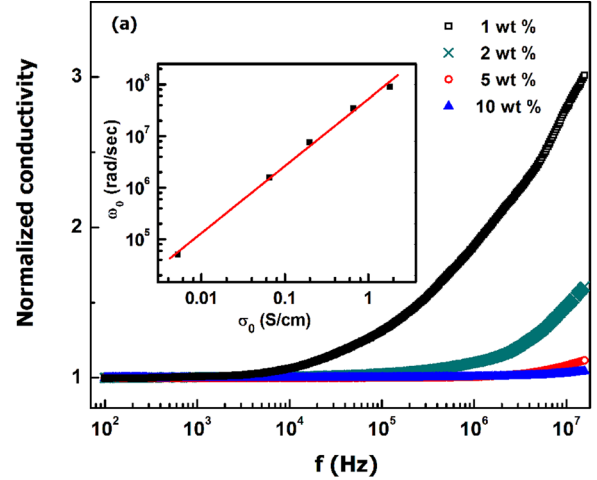


FIG. 6. (a) Normalized ac conductivity for different sMWNT weight fraction at 300 K. Inset shows the variation of onset frequency with respect to the dc conductivity (σ_0). (b) Normalized conductivity vs. frequency for 1 wt. % composite at various temperatures. Inset: frequency exponent (s) vs. T and the solid line is fit to Eq. (4). (c) Normalized conductivity vs. frequency for 10 wt. % composite at various temperatures.

where a_1 is the coefficient of forward interference effects, a_2 is the coefficient of wave function shrinkage term, and a_3 accounts for the contribution from scattering effects at very low fields.²⁶ A fit to the experimental data is carried out using Eq. (3), as in Fig. 5. The temperature dependence of the coefficient of linear negative MR term (a_1) is shown in the inset of Fig. 5, in a log-log scale. The linear dependence suggests that the scattering process is reasonably within the weak limit.²⁶ Schrimacher has shown that a_1 follows T^{-s} behaviour, and the exponent s is sensitive to the nature of disorder and dimensionality involved in the transport.²⁷ The fit in the inset of Fig. 5 yields $s = 0.81 \pm 0.02$, a value slightly lower than the theoretically predicted ($s = 0.87$) for 3D VRH.

The ac conductivity measurements were carried out in sMWNT-Nafion composites to obtain additional information about the charge transport. While dc conductivity follows VRH model, the effect of disorder on the ac conductivity is expected to be even more significant, as observed in various disordered systems.^{28,29} The frequency dependence of conductivity at various sMWNT loading, at room temperature, is shown in Fig. 6(a). The data are normalized with dc conductivity (σ_0) values to find out the relative response. The conductivity remains nearly constant for all the composites, up to a characteristic frequency, called the onset frequency ω_0 , and starts to increase at higher frequencies, as typically observed in many disordered systems.^{28,29} The ac conductivity follows a power law: $\sigma(\omega) = A\omega^s$, where A is a constant dependent on temperature and s is an exponent dependent on both frequency and temperature.²⁸ For our system, we define the onset of frequency as the value where $\sigma(\omega_0) = 1.05\sigma_0$, where σ_0 is the dc conductivity. The measured onset frequency was found to increase with its dc conductivity values, as shown in the inset of Fig. 6(a). The log-log plot suggests a relation between the onset frequency and dc conductivity values: $\omega_0 \sim \sigma_0^a$, where $a \sim 1$.³⁰ It has been observed that the onset frequency ω_0 increases by several orders of magnitude as the sMWNT content is increased, and this is found to be consistent with percolative transport mechanism.³¹

The frequency dependent ac measurements are more sensitive to local variations in the network than dc measurements, since the aggregation of nanotubes affects the ac measurements.³¹ In any disordered system, a correlation length λ can be defined which corresponds to the distance between connections (e.g., junctions and nodes) in the system.³¹ The ac conductivity measurement at a given frequency probes a typical length scale. At low frequencies, carriers travel long distances and hence the probed distance will be longer. Whereas at higher frequencies, carriers travel short distances and the probed length scale is shorter. It has

been shown for carriers in disordered systems exhibiting a random walk motion, the probed length scale as $L_\omega \propto \omega^{-1/2}$, especially in the absence of a dc bias electric field.³¹ At the onset frequency ω_0 , the carrier travels a distance $\sim \lambda$. A higher value for the onset frequency implies smaller correlation length and shorter connections in the system.^{32,33} At low frequency, $L_\omega > \lambda$, the probed length contains multiple CNT junctions that cause an increase in resistance, since the junction offers larger resistance than individual tube resistance. As the frequency increases, L_ω becomes smaller than λ , as a result the measured conductance increases due to the reduction in junction resistance. Whereas at very high frequencies, the probed length scales can be reduced to intratube length, and the ac response becomes independent of the CNT weight percentage.

Several theories have been proposed to describe the high frequency ac charge transport process in disordered materials.^{28,29} It is commonly assumed that the pair approximation model holds, and the carrier motion is assumed to be localized within pairs of sites, which is the high frequency limit of the general case, and in this mechanism multiple hopping can occur among the sites within a cluster.³⁴ Essentially, two distinct processes have been proposed for the relaxation mechanism, namely quantum mechanical tunneling and classical hopping over a barrier, or a combination or variant of the two.^{28,29} To find out the relaxation mechanism, temperature dependence of ac conductivity has to be examined in detail. The variation of ac conductivity of 1 wt. % sMWNT sample at different temperatures is presented in Fig. 6(b). The variation of s as a function of temperature is shown in the inset of Fig. 6(b). The value of s increases with decrease of temperature. A more detailed analysis of the temperature dependence of s shows that the frequency response follows the CBH model. In CBH model, the carriers hop between sites over the potential barriers, with some extent of correlation.²⁹ The frequency exponent s in this model is given by²⁹

$$s = 1 - \frac{6k_B T}{W_M + k_B T \ln(\omega \tau_0)}, \quad (4)$$

where W_M is the effective barrier height and τ_0 is the relaxation time. The data in the inset of Fig. 6(b) fit quite well to Eq. (4), and the fit parameters are $W_M = 0.23$ eV and $\tau_0 = 8.64 \times 10^{-7}$ s (at $\omega = 6.28 \times 10^6$ rad s⁻¹). The ac conductivity data of 10 wt. % sample, at various temperatures down to 4.2 K, are shown in Fig. 6(c). It is clearly seen that there is hardly any significant change in conductivity even at 4.2 K, while compared to that in 1 wt. % sample. The improved ac transport in 10 wt. % sample could be due to the

TABLE I. Comparison of transport parameters for 1 and 10 wt. % samples of sMWNT-Nafion composites.

Nafion-sMWNT (wt. %)	Conductivity at 300 K (S/cm)	Resistivity ratio ($\rho_6 \text{ K} / \rho_{300 \text{ K}}$)	Low temperature transport exponent p	T_0 (K)	AC conductivity onset frequency at 300 K (MHz)	Connectivity length scale L_E (nm)
1	0.005	70	0.28	38 500	8×10^{-3}	~ 80
10	3.2	5	0.24	560	> 16	~ 806

increase in sMWNT loading well above the percolation threshold. Further, this could also give an insight into the quality of sMWNT dispersion as at higher frequencies aggregation of CNTs can lead to increase in conductivity as the ac probe length scale becomes shorter.³² However, a more controlled study is required to distinguish between the roles of CNT loading and dispersion on the ac conductivity of nanocomposite systems. A comparison of the charge transport parameters for 1 and 10 wt. % of sMWNT samples is summarized in Table I.

IV. CONCLUSIONS

In summary, we have investigated the charge transport properties of functionalized multi-wall carbon nanotube-Nafion composites. The functionalization of MWNT is found to be effective in preventing nanotube aggregation and helps to better disperse MWNTs within Nafion. The dc conductivity of composites shows a percolation threshold at $p_c = 0.42$ wt. %, and the critical exponent, $t = 2.13$. The low temperature transport properties at different sMWNT content, one close to the percolation threshold and another well above the threshold, are studied in detail. In both 1 and 10 wt. % samples, 3D Mott VRH is observed. The magneto-transport measurements at low temperatures indicate the interplay of forward interference mechanism (negative MR) and wave-function shrinkage (positive MR) in 10 wt. % sample, and the carrier scattering is observed to be in the weak limit. The extent of sMWNT network connectivity is further probed by high electric-field and high frequency measurements. The value of L_E shows an order of magnitude difference between 1 and 10 wt. % composites. The ac conductivity in 1 wt. % sample follows a power law: $\sigma(\omega) = A\omega^s$, and s decreases with increasing temperature as expected in the CBH model. The nanoscopic transport parameters together with the morphology are quite useful in optimizing the charge transport properties in sMWNT-Nafion.

ACKNOWLEDGMENTS

The low temperature high magnetic field measurements were carried out at the DST National facility for Low Temperature and High Magnetic Field, IISc, Bangalore (the authors thank Dr. V. Prasad). C.S.S.S. acknowledges CSIR, New Delhi for financial assistance. R.K. thanks UGC for financial support, and V.K.P. acknowledges CSIR for funding this work.

- ¹B. J. Landi, R. P. Raffaele, M. J. Heben, J. L. Alleman, W. VanDerveer, and T. Gennett, *Nano Lett.* **2**, 1329 (2002).
- ²R. Kannan, B. A. Kakade, and V. K. Pillai, *Angew. Chem., Int. Ed.* **47**, 2653 (2008).
- ³C. Wang, M. Waje, X. Wang, J. M. Tang, R. C. Haddon, and Yan, *Nano Lett.* **4**, 345 (2003).
- ⁴M. Moniruzzaman and K. I. Winey, *Macromolecules* **39**, 5194 (2006).
- ⁵J. N. Coleman, S. Curran, A. B. Dalton, A. P. Davey, B. McCarthy, W. Blau, and R. C. Barklie, *Phys. Rev. B* **58**, R7492 (1998).
- ⁶S. Barrau, P. Demont, A. Peigney, C. Laurent, and C. Lacabanne, *Macromolecules* **36**, 5187 (2003).
- ⁷E. Kymakis and G. A. J. Amaratunga, *J. Appl. Phys.* **99**, 084302 (2006).
- ⁸R. Ramasubramaniam, J. Chen, and H. Liu, *Appl. Phys. Lett.* **83**, 2928 (2003).
- ⁹E. Kymakis, I. Alexandou, and G. A. J. Amaratunga, *Synth. Met.* **127**, 59 (2002).
- ¹⁰H. M. Kim, M.-S. Choi, J. Joo, S. J. Cho, and H. S. Yoon, *Phys. Rev. B* **74**, 054202 (2006).
- ¹¹N. G. Sahoo, S. Rana, J. W. Cho, L. Li, and S. H. Chan, *Prog. Polym. Sci.* **35**, 837 (2010).
- ¹²R. Kannan, M. Parthasarathy, S. U. Maraveedu, S. Kurungot, and V. K. Pillai, *Langmuir* **25**, 8299 (2009).
- ¹³J. N. Coleman, U. Khan, W. J. Blau, and Y. K. Gun'ko, *Carbon* **44**, 1624 (2006).
- ¹⁴M. Jaiswal, W. Wang, K. A. S. Fernando, Y. P. Sun, and R. Menon, *J. Phys.: Condens. Matter* **19**, 446006 (2007).
- ¹⁵J.-M. Thomassin, J. Kollar, G. Caldarella, A. Germain, R. Jérôme, and C. Detrembleur, *J. Membr. Sci.* **303**, 252 (2007).
- ¹⁶Y.-L. Liu, Y.-H. Su, C.-M. Chang, Suryani, D.-M. Wang, and J.-Y. Lai, *J. Mater. Chem.* **20**, 4409 (2010).
- ¹⁷D. Stauffer and A. Aharony, *Introduction to Percolation Theory* (Taylor and Francis, London, 1994).
- ¹⁸C. O. Yoon, M. Reghu, D. Moses, A. J. Heeger, Y. Cao, T. A. Chen, X. Wu, and R. D. Rieke, *Synth. Met.* **75**, 229 (1995).
- ¹⁹B. I. Shklovskii, *Sov. Phys. Semicond.* **6**, 1964 (1973).
- ²⁰M. Jaiswal, C. S. S. Sangeeth, and R. Menon, *Appl. Phys. Lett.* **95**, 032111 (2009).
- ²¹M. S. Fuhrer, M. L. Cohen, A. Zettl, and V. Crespi, *Solid State Commun.* **109**, 105 (1998).
- ²²D. Jana and J. Fort, *Physica B* **344**, 62 (2004).
- ²³M. Reghu, K. Väkiparta, Y. Cao, and D. Moses, *Phys. Rev. B* **49**, 16162 (1994).
- ²⁴V. L. Nguyen, B. Z. Spivak, and B. I. Shklovskii, *Sov. Phys. JETP* **62**, 1021 (1985).
- ²⁵R. Rosenbaum, T. Murphy, E. Palm, S. Hannahs, and B. Brandt, *Phys. Rev. B* **63**, 094426 (2001).
- ²⁶M. E. Raikh and G. F. Wessels, *Phys. Rev. B* **47**, 15609 (1993).
- ²⁷W. Schirmacher, *Phys. Rev. B* **41**, 2461 (1990).
- ²⁸A. R. Long, *Adv. Phys.* **31**, 553 (1982).
- ²⁹S. R. Elliot, *Adv. Phys.* **36**, 135 (1987).
- ³⁰J. C. Dyre and T. B. Schröder, *Rev. Mod. Phys.* **72**, 873 (2000).
- ³¹B. E. Kilbride, J. N. Coleman, J. Fraysse, P. Fourmet, M. Cadek, A. Drury, S. Hutzler, S. Roth, and W. J. Blau, *J. Appl. Phys.* **92**, 4024 (2002).
- ³²C. S. S. Sangeeth, M. Jaiswal, and R. Menon, *J. Phys.: Condens. Matter* **21**, 072101 (2009).
- ³³C. S. S. Sangeeth, P. Jimenez, A. M. Benito, W. K. Maser, and R. Menon, *J. Appl. Phys.* **107**, 103719 (2010).
- ³⁴A. Ghosh, *Phys. Rev. B* **41**, 1479 (1990).
- ³⁵See supplementary material at <http://dx.doi.org/10.1063/1.4749264> for XPS measurements on sMWNT and SEM images of pristine MWNT and sMWNT-Nafion composites.